ChemComm

COMMUNICATION

View Article Online
View Journal | View Issue

Cite this: *Chem. Commun.*, 2024, **60**, 1023

Received 25th October 2023,
Accepted 20th December 2023

DOI: 10.1039/d3cc05247h

rsc.li/chemcomm

Highly branched bolapolyphilic liquid crystals with a cubic A15 network at the triangle-square transition†

Christian Anders, [a] Matthias Wagner,[a] Mohamed Alaasar, [a] Virginia-Marie Fischer,[b] Rebecca Waldecker, [b] Yangyang Zhao, [c] Tianyi Tan, [c] Yu Cao, *[c] Feng Liu [c] and Carsten Tschierske *[a]

Rod-like bolapolyphiles with highly branched carbosilane-based side-chains self-assemble into several honeycomb structures if the oligo(*p*-phenylene ethynylene) core is polyfluorinated, whereas for the non-fluorinated series an A15 type cubic network of rod-bundles was observed instead, suggesting a brand new pathway for the transition between triangular and square honeycomb phases.

Liquid crystalline (LC) systems represent perfect examples to show how nature creates well-defined structures by soft matter self-assembly.[1,2] Particularly successful examples are provided by T-shaped[3] and X-shaped bolapolyphilic block molecules (Fig. 1h),[3–5] *i.e.* amphiphiles with two polar ends at a lipophilic unit and combining more than two incompatible units. These molecules are composed of a π-conjugated rod with sticky hydrogen bonding at both ends and flexible side-chains. Depending on the rod-length, side-chain number, length and volume, these molecules form a wide range of columnar liquid crystalline phases with honeycomb structures (Fig. 1). In the honeycombs, the π-conjugated rod-like cores lie perpendicular to the column long axis, held together at the edges by columns involving the hydrogen bonded glycerol ends. The resulting prismatic cells are filled by the flexible side-chains. Depending on the side-chain volume and the length of the rigid rod-like core, different types of honeycombs were observed, such as triangular, square, pentagonal, and hexagonal, while compounds with even larger chains tend to form giant honeycombs,[6] lamellar phases[7] and cubic network structures (see also Section S3.1, ESI†).[8]

The transition from triangular ($Col_{hex}/p6mm$) to square honeycombs ($Col_{squ}/p4mm$, Fig. 1a and g) is of particular interest owing to the large cell volume jump between them and the huge number of possible tiling patterns involving rectangular[9] and rhombic cells (Fig. 1b and f)[10] as well as combinations of squares with equilateral triangles (Fig. 1c and d),[11,12] the latter being of special interest as they could possibly provide a source of liquid quasicrystals.[13]

While in previous work linear and simply branched alkyl chains have been used (Fig. 1h and i), we discuss here, for the first time, bolapolyphiles with triply branched side-chains (Fig. 1j), where silicon acts as branching point.[14] An oligo(*p*-phenylene ethynylene) (OPE) unit was used as rod-like core,[4,5,10,15,16] and the total chain volume was chosen to fit into the triangle-square transition region. The volume was

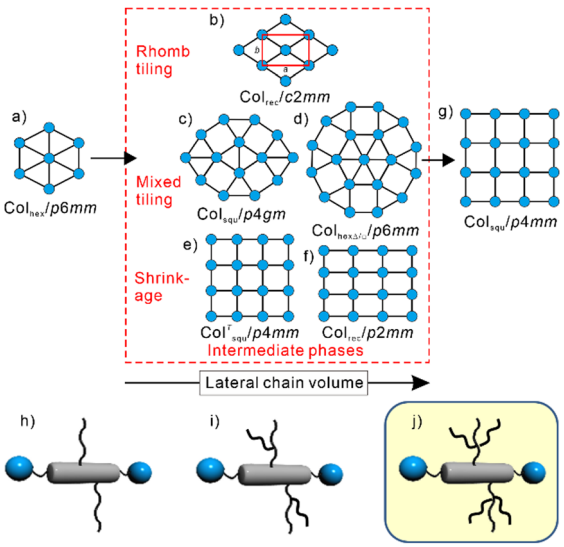

Fig. 1 (b)–(f) Selected intermediate phases at the transition between (a) triangular and (g) square LC honeycombs; the shown nets represent cuts through the honeycombs perpendicular to the *c*-axis (see Fig. 3c.i for spatial models), the rod-like cores are organized along the dark lines and the blue dots represent the polar columns of the end groups, the side chains fill the cells; (h) and (i) bolapolyphiles forming these tiling patterns and (j) compounds under discussion herein.

[a] *Institute of Chemistry, Martin Luther University Halle-Wittenberg, Kurt-Mothes Str. 2, Halle 06120, Germany. E-mail: Carsten.tschierske@chemie.uni-halle.de*
[b] *Institute of Mathematics, Martin Luther University Halle-Wittenberg, Theodor-Lieser-Str. 5, Halle 06120, Germany*
[c] *Shaanxi International Research Center for Soft Matter, Xi'an Jiaotong University, Xi'an 710049, P. R. China. E-mail: yu.cao@xjtu.edu.cn*

† Electronic supplementary information (ESI) available: Synthesis, methods, analytical data, additional data and discussions. See DOI: https://doi.org/10.1039/d3cc05247h

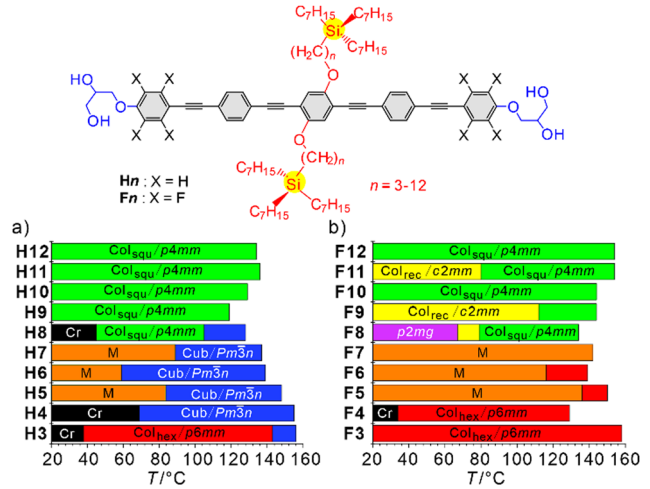

Fig. 2 Molecular structure and LC phases of (a) **H*n*** and (b) **F*n*** as observed on cooling with 10 K min^{-1}; abbreviations: Cr = crystalline solid; Col$_{hex}$/*p6mm* and Col$_{squ}$/*p4mm* = triangular and square LC honeycombs, respectively; Col$_{rec}$/*c2mm* and *p2mg* = tilings by rhombic and non-regular triangular honeycombs, respectively; Cub/*Pm*$\bar{3}$*n* = cubic network phase with *Pm*$\bar{3}$*n* space group; M = unknown LC phases; isotropic liquid is at the right side of the columns; for numerical data, transitions on heating and enthalpies, see Table S1a, b, for DSCs Fig. S1 and S2, for textures Fig. S3–S6, for SAXS/WAXS data Fig. S7–S10, Tables S2–S29 (ESI†).

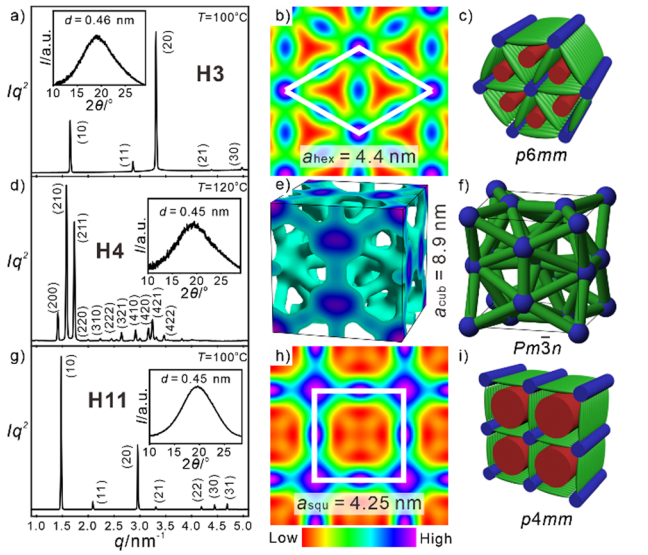

Fig. 3 (a), (d) and (g) SAXS diffractograms with WAXS (insets), (b), (e) and (h) reconstructed ED maps, and (c), (f) and (i) schematic illustrations of the organization of the molecules in the (a)–(c) Col$_{hex}$/*p6mm* phase of **H3** at T = 100 °C; (d)–(f) Cub/*Pm*$\bar{3}$*n* phase of **H4** at T = 120 °C and (g)–(i) Col$_{squ}$/*p4mm* phase of **H11** at T = 100 °C.

fine-tuned by modifying the spacer unit between core and tri-*n*-heptylsilyl unit from n = 3 to 12. Two series were studied, the non-fluorinated compounds **H*n*** (X = H) and the compounds **F*n*** with the outer benzene rings being perfluorinated (X = F). The synthesis is described in Scheme S2 and Section S4 (ESI†), and investigation was conducted by differential scanning calorimetry (DSC), polarized optical microscopy (POM) and small- and wide-angle X-ray scattering (SAXS, WAXS) as described in Section S1 (ESI†).

Three different LC phases were observed for the series **H*n*** (Fig. 2a). Compound **H3** with the shortest spacer forms a hexagonal columnar phase with a_{hex} = 4.3 nm between 70 and 147 °C (Fig. 3a). The lattice parameter corresponds to the molecular length (L_{mol} = 4.0–4.4 nm, depending on the conformation of the glycerol groups), suggesting a triangular honeycomb as confirmed by the reconstructed electron density (ED) map in Fig. 3b, showing triangular low ED regions (red/yellow) filled by the aliphatic side-chains which are separated by medium electron density walls (green) of the OPE cores and high ED dots (purple/blue) involving the glycerol groups at the junctions. The number of molecules in each unit cell with an assumed height of h = 0.45 nm is n_{cell} = 3.2, meaning that a single rod-like core is found in the lateral cross section of the walls (n_{wall} = n_{cell}/3; Table S27, ESI†). The diffuse character of the WAXS (insets in Fig. 3a, d and g) indicates the absence of fixed positions of individual molecules, thus confirming a highly dynamic LC honeycomb. Upon heating to 147 °C a transition to a viscous optically isotropic mesophase is observed, which becomes fluid at 160 °C. This transition is associated with an enthalpy of 1.5 kJ mol^{-1}, indicating a cubic mesophase occurring between 147 and 160 °C (Fig. S1a, ESI†).

For the next homologue **H4** the range of this cubic mesophase is expanded and the triangular honeycomb is completely removed. With further growing n it is retained up to n = 8 (Fig. 2a). All cubic mesophases show the same typical pattern of three strong peaks in the SAXS (Fig. 3d) indicative for the (200), (210) and (211) reflections of a *Pm*$\bar{3}$*n* lattice; the WAXS is diffuse, confirming the LC state. This type of cubic LC phase was recently analysed in detail for a series of compounds related to **H*n***, but having two simply branched alkyl chains (see Fig. 1i and Scheme S1 and discussion in Section S3.2, ESI†).[17] The *Pm*$\bar{3}$*n* phase, shown in Fig. 3e and g, is formed by a network of rod-bundles interconnected at the junctions by spheres or oblate spheroids involving the polar glycerol groups while the continuum is filled by the side chains. The positions of the spheres at the edges, in the centre, and pairs of spheroids on the 6 faces of the unit cell corresponds to that observed for the A15 Frank Kasper phases,[18] however, in this case representing a dense packing of tetrahedra formed by bundles of rods interconnected by the glycerol spheres/spheroids at the edges. The lattice parameter a_{cub} = 8.6–9.2 nm, increases with growing n from 3 to 6 and then remains almost constant, and 5–6 molecules are organized in the cross-section of the bundles of single molecular length (Table S28, ESI†).[17]

For compounds **H*n*** with n = 5–8 the cubic phase is accompanied by birefringent mesophases at lower temperature (Fig. S3c and d, ESI†) and for the following homologues with n = 9–12 the cubic phase is completely removed. For compounds **H5–H7** a complicated diffraction pattern (M) is found, which needs to be solved in future work. In contrast, a simple square lattice with *p4mm* plane group and a_{squ} = 4.1–4.3 nm (Fig. 3g), again corresponding to the molecular length, is observed for **H8–H12** (Table S29, ESI†). This indicates a square honeycomb, as also obvious from the ED map

(Fig. 3h and i). No further transition is observed for the Col_{squ} phases until crystallization.

The interesting and new observation in the series of compounds **H*n*** depending on the spacer length *n* is, that a cubic phase occurs at the transition between two columnar LC phases, only having different honeycomb shapes. This means that it is not preliminary caused by changing interface curvatures, but by a destabilization of the honeycombs due to steric and geometric frustration during the triangle-square transition. Hence, it is a new intermediate structure at this transition (see also Section S3.2, ESI†).[12]

The situation changes for the series of core-fluorinated compounds **F*n*** where the $Pm\bar{3}n$ phase is completely removed (Fig. 2b and Tables S1a, b, ESI†), while the range of the triangular honeycomb with *p6mm* plane group is expanded up to $n = 6$, indicating that a bit more space is available in the polygonal cells formed by compounds **F*n***. The lattice parameters of the Col_{hex} and Col_{squ} phases (a_{hex} = 4.1–4.3 nm, a_{squ} = 4.2–4.4 nm) are almost identical to those observed for the series **H*n*** (Tables S27, S29, ESI†). There is a general mesophase stabilization by core fluorination, with a tendency to increase with growing side chain length (Fig. 2). There is also an odd–even effect of the spacer length with a tendency to higher mesophase stabilities for compounds with odd numbered *n* (or an even total numbers of connecting atoms $n + 1$ including the ether oxygen). This is because of the effect of spacer parity on the side chain conformation (linear *vs.* bent, Fig. S16, ESI†) which modulates the packing of the bulky trialkylsilyl end group. This leads to a non-continuous development of the phase stabilities, lattice types, and lattice parameters depending on *n*, and to a more complicated sequence of different LC phases for the series **F*n***. The WAXS is still diffuse for all the mesophases, thus representing true LCs (Fig. 4c, f and Fig. S8, ESI†).

There are additional mesophases accompanying the square honeycombs of some of the compounds **F8–F12** at lower temperature (Fig. 2b). Upon cooling the *p4mm* phase of compound **F8** a LC phase with centred rectangular lattice and *c2mm* plane group is formed below 80 °C (Fig. 4a–c). The ED map in Fig. 4b shows a honeycomb based on rhombic cells with $a = 5.0$ and $b = 7.0$ nm, *i.e.* a distorted square honeycomb, formed by 4.3 nm long walls. On cooling it is followed below 64 °C by a further change of the SAXS pattern which can now be indexed to a *p2mg* lattice (Fig. 4d–f, Table S20, ESI†). The ED map shows that this honeycomb is composed of acute triangular cells where two walls are slightly expanded to 4.5 nm while the third is 4.0 nm. Optical investigations support the proposed phase structures (see Fig. S5, ESI†). The transition *p4mm* → *c2mm* is attributed to an increasing contribution of *all-trans* alkyl chains conformations at lower temperature, which prefer rhombic cells for easier chain expansion, while division of the rhombi into two triangles at the *c2mm* → *p2mg* transition is attributed to the simultaneously occurring shrinkage of the side chain volume due to reduced thermal motions.

While the following homologues **F10** and **F12** with even numbered *n* form exclusively the square honeycomb, for the odd numbered **F9** and **F11** the *c2mm* phase is found and gradually suppressed with growing *n* by the *p4mm* phase (Fig. 2b). For the *p4mm* phases, the side lengths of 4.1–4.3 nm corresponds to L_{mol}, making any tilted organization of the rods in the honeycomb walls unlikely, even at low temperature to about 40 °C (Table S29 and Fig. S15, ESI†). However, in the *c2mm* phase of **F9** the side length starts decreasing from 4.2 nm around 80 °C to 3.95 nm at 40 °C, indicating the development of a small tilt due to continuing side chain volume shrinkage upon cooling (see Fig. S14, ESI†). This tilt shrinks the rhombi of **F9** without splitting into two triangles as observed for **F8**.

Here the question of the origin of the effects of core fluorination on the LC self-assembly arises, which can be subdivided into steric and polar effects. The larger size of F (0.13 nm^3) compared to H (0.07 nm^3, crystal volume increments)[19] can reduce or increase the space available for the side-chains, depending on the preferred orientation of the planes of the benzene rings (Fig. 5a–c). Benzenes aligned with their faces perpendicular to the column axis (Fig. 5c) reduce the available space by fluorination due to the reduced height *h* of the (hypothetical) 3D unit cell along the π-stacking direction and by the accommodation of the larger fluorines inside the prismatic cells. Benzene rings aligned almost parallel or only slightly tilted to the *c*-direction increase *h* and thus provide additional space if H is replaced by F (Fig. 5b). Though there is still an almost free rotation of the OPEs in the honeycomb walls, the polar effects influence the preferred orientation of the π-planes along the honeycomb walls by electrostatic interactions. Compounds **H*n***, having electron rich benzenes, for which only one diffuse SAXS around 0.45 nm is observed in all LC phases (Fig. 3a, d and g and Fig. S7, ESI†), are known to

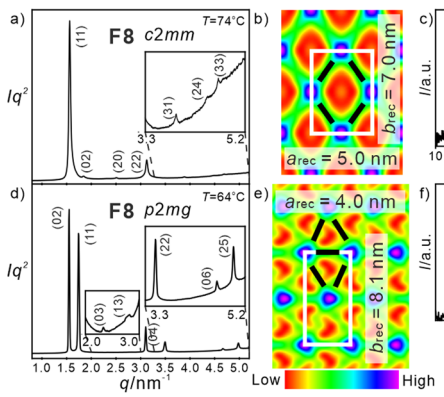

Fig. 4 SAXS diffractograms (left) with WAXS (right), and reconstructed ED maps (middle) of the honeycomb phases of compound **F8** (see Tables S18–S20, ESI†).

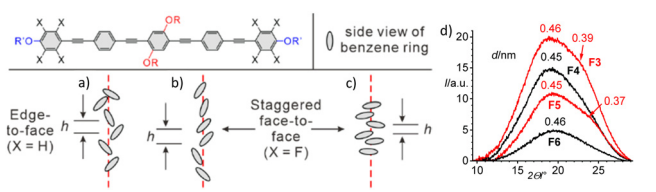

Fig. 5 (a)–(c) Schematic presentation of the stacking modes in the honeycomb walls; the grey ellipses represent side view on the benzene rings if viewed along the OPE long axis; the red dashed line is the *c*-axis and *h* the intermolecular stacking distance; (d) shows the odd–even effect of the WAXS of compounds **F3–F6** at 120 °C; intensities are not scaled.

prefer an edge-to-face orientation (Fig. 5a and Fig. S17a, ESI†), while the electron deficit π-systems of the perfluorinated rings in **F*n*** tend to align face-to-face (Fig. 5b and c).[20] This difference is evident in the WAXS profiles of compounds **F*n*** where a weak broad shoulder around 0.36–0.39 nm is found beside the diffuse scattering maximum at 0.44–0.46 nm (Fig. 4c, f and 5d and Fig. S8, ESI†). The very broad and weak shoulder indicates a poor order and short correlation length of π-stacking as found in the stacking mode in Fig. 5b, while that in Fig. 5c is expected to lead to a stronger scattering. This additional scattering is the strongest for compounds **F*n*** with odd-numbered *n* (see Fig. 5d). This odd–even effect becomes weaker with growing *n* and the intensity of the shoulder rises with lowering temperature (Fig. S8, ESI†). Face-to-face stacking is known to preferably take place by alternation of the electron-rich benzenes or acetylenes and the polyfluorinated benzenes,[20] which in our case would lead to a significant longitudinal shift between the cores, causing a tilt of the rods in the walls, thus reducing the effective value of L_{wall} of the honeycombs (Fig. S17b–d, ESI†).[15,16] However, this shift would distort the segregation of the polar glycerols from the aromatic cores. In the present case the reduction of L_{wall} due to this mode of tilting is not observed in most cases (except *c2mm* of **F9**, see above) and a face-to-face packing of the electron deficit fluorinated rings with some transversal shift appears more likely (Fig. 5b, c and Fig. S17e, ESI†).[21] This face-to-face stacking increases the core–core attractive interactions, thus supporting the quasi infinite stacking along the honeycomb walls. This provides a higher stability for the honeycombs (and the M phase) of compounds **F*n*** and favours the honeycombs over the shorter stacks in the $Pm\bar{3}n$ networks of compounds **H3–H8**. The transversal shifted face-to-face stacking increases *h* if the benzenes preferably arrange with their planes parallel to the honeycomb main axis (see Fig. 5b), thus leading to more space for the side-chains and this shifts the triangle → square transition towards larger chain volume (**H3** → **F8**), in line with the experimental observations. This packing mode is obviously supported by odd-numbered *n* (**F9**, **F11**), favouring the formation of the smaller rhombic honeycombs replacing the larger square of the even numbered compounds **F10** and **F12**.

In summary, a new type of polyphilic block-molecules with highly branched carbosilane-based side-chains is reported. For the non-fluorinated series an A15-type cubic network phase composed of tetrahedra of rod-bundles was observed as a new mode of transition between triangular and square honeycombs. Peripheral core fluorination was found to be an efficient tool to suppress the $Pm\bar{3}n$ network formation and provides triangular and rhombic honeycombs with reduced symmetry. This could pave the way towards new periodic and quasiperiodic honeycombs based on mixed triangle/square tilings.[11,12] If the unknown M phase belongs to these complex honeycombs or represents another complex tiling by rod-bundles remains to be investigated in future work.

This work was supported by the Deutsche Forschungsgemeinschaft (436494874 – RTG 2670), the National Natural Science Foundation of China (No. 21761132033, 21374086, and 12204369), Science and Technology Agency of Shaanxi Province (2023-YBGY-459), China Postdoctoral Science Foundation (2022M712551, 2023T160505). The authors are grateful to Beamline BL16B1 at SSRF (Shanghai Synchrotron Radiation Facility, China) for providing the beamtimes and to V. Adjedje and S. Tanner Dept. of Macromol. Chem., MLU Halle for HR-MS investigations.

Conflicts of interest

There are no conflicts to declare.

Notes and references

1 T. Kato, J. Uchida, T. Ichikawa and T. Sakamoto, *Angew. Chem., Int. Ed.*, 2018, **57**, 4335; M. Lehmann, M. Dechant, M. Lambov and T. Ghosh, *Acc. Chem. Res.*, 2019, **52**, 1653; J. W. Goodby, S. J. Cowling, C. K. Bradbury and R. J. Mandle, *Liq. Cryst.*, 2022, **49**, 908; J. Voskul and M. Giese, *Aggregate*, 2023, **3**, e124; H. K. Bisoyi and Q. Li, *Chem. Rev.*, 2022, **122**, 4887.
2 R. Zhang, Z. Su, X.-Y. Yan, J. Huang, W. Shan, K.-H. Dong, X. Feng, Z. Lin and S. Z. D. Cheng, *Chem. – Eur. J.*, 2020, **26**, 6741.
3 (*a*) C. Tschierske, *Chem. Soc. Rev.*, 2007, **36**, 1930; (*b*) C. Tschierske, C. Nürnberger, H. Ebert, B. Glettner, M. Prehm, F. Liu, X. B. Zeng and G. Ungar, *Interface Focus*, 2012, **2**, 669; (*c*) Y. Sun and F. A. Escobedo, *J. Chem. Theory Comput.*, 2023, DOI: 10.1021/acs.jctc.3c00395.
4 M. Poppe, C. Chen, H. Ebert, S. Poppe, M. Prehm, C. Kerzig, F. Liu and C. Tschierske, *Soft Matter*, 2017, **13**, 4381.
5 S. Poppe, M. Poppe, H. Ebert, M. Prehm, C. Chen, F. Liu, S. Werner, K. Bacia and C. Tschierske, *Polymers*, 2017, **9**, 471.
6 A. Scholte, S. Hauche, M. Wagner, M. Prehm, S. Poppe, C. Chen, F. Liu, X. Zeng, G. Ungar and C. Tschierske, *Chem. Commun.*, 2020, **56**, 62.
7 M. Prehm, C. Enders, X. Mang, X. Zeng, F. Liu, G. Ungar, U. Baumeister and C. Tschierske, *Chem. – Eur. J.*, 2018, **24**, 16072.
8 X. Zeng, S. Poppe, A. Lehmann, M. Prehm, C. Chen, F. Liu, H. Lu, G. Ungar and C. Tschierske, *Angew. Chem., Int. Ed.*, 2019, **58**, 7375; S. Poppe, X. Cheng, C. Chen, X. Zeng, R.-B. Zhang, F. Liu, G. Ungar and C. Tschierske, *J. Am. Chem. Soc.*, 2020, **142**, 3296; C. Chen, M. Poppe, S. Poppe, C. Tschierske and F. Liu, *Angew. Chem., Int. Ed.*, 2020, **59**, 20820; X. Cai, S. Hauche, S. Poppe, Y. Cao, L. Zhang, C. Huang, C. Tschierske and F. Liu, *J. Am. Chem. Soc.*, 2023, **145**, 1000.
9 A. Lehmann, A. Scholte, M. Prehm, F. Liu, X. Zeng, G. Ungar and C. Tschierske, *Adv. Funct. Mater.*, 2018, **28**, 1804162.
10 A. Saeed, M. Poppe, M. B. Wagner, S. Hauche, C. Anders, Y. Cao, L. Zhang, C. Tschierske and F. Liu, *Chem. Commun.*, 2022, **58**, 7054.
11 M. Poppe, C. Chen, S. Poppe, F. Liu and C. Tschierske, *Commun. Chem.*, 2020, **3**, 70.
12 X. Cheng, H. Gao, X. Tan, X. Yang, M. Prehm, H. Ebert and C. Tschierske, *Chem. Sci.*, 2013, **4**, 3317.
13 X. Zeng, B. Glettner, U. Baumeister, B. Chen, G. Ungar, F. Liu and C. Tschierske, *Nat. Chem.*, 2023, **15**, 625; Y. Cao, A. Scholte, M. Prehm, C. Anders, C. Chen, J. Song, L. Zhang, G. He, C. Tschierske and F. Liu, *Angew. Chem., Int. Ed.*, 2023, e202314454; M. Imperor-Clerc, A. Jagannathan, P. Kalugin and J.-F. Sadoc, *Soft Matter*, 2021, **17**, 9560; U. Tu Lieu and N. Yoshinaga, *Soft Matter*, 2022, **18**, 7497.
14 A. Kreyes, A. Masoud, I. Lieberwirth, R. Mauer, F. Laquai, K. Landfester and U. Ziener, *Chem. Mater.*, 2010, **22**, 6453.
15 M. Poppe, C. Chen, F. Liu, M. Prehm, S. Poppe and C. Tschierske, *Soft Matter*, 2017, **13**, 4676.
16 (*a*) M. Poppe, C. Chen, S. Poppe, C. Kerzig, F. Liu and C. Tschierske, *Adv. Mater.*, 2020, 202005070; (*b*) M. Poppe, C. Chen, F. Liu, S. Poppe and C. Tschierske, *Chem. Commun.*, 2021, **57**, 6526.
17 C. Chen, M. Poppe, S. Poppe, M. Wagner, C. Tschierske and F. Liu, *Angew. Chem., Int. Ed.*, 2022, e202203447.
18 (*a*) K. Borisch, S. Diele, P. Göring and C. Tschierske, *Chem. Commun.*, 1996, 237; (*b*) V. S. K. Balagurusamy, G. Ungar, V. Percec and G. Johannsson, *J. Am. Chem. Soc.*, 1997, **119**, 1539; (*c*) K. D. Dorfman, *Macromolecules*, 2021, **54**, 10251.
19 A. Immirzi and B. Perini, *Acta Cryst. Sect. A*, 1977, **33**, 216.
20 (*a*) C. A. Hunter and J. K. M. Sanders, *J. Am. Chem. Soc.*, 1990, **112**, 5525; (*b*) G. A. Coates, A. R. Dunn, L. M. Henling, D. A. Dougherty and R. H. Grubbs, *Angew. Chem., Int. Ed. Engl.*, 1997, **36**, 248; (*c*) K. Kishikawa, *Isr. J. Chem.*, 2012, **52**, 800.
21 M.-M. Zhou, J. He, H.-M. Pan, Q. Zeng, H. Lin, K.-Q. Zhao, P. Hu, B.-Q. Wang and B. Donnio, *Chem. – Eur. J.*, 2023, 3202301829.

